Article

High-speed 0.22 THz communication system with 84 Gbps for real-time uncompressed 8K video transmission of live events

Ke Liu [1], Yinian Feng [2,4] ✉, Chong Han [3,4] ✉, Bo Chang [1,4], Zhi Chen [1,4] ✉, Zicheng Xu[1], Lingxiang Li[1], Bo Zhang [2] ✉, Yihui Wang[2] & Qiang Xu[1]

Terahertz frequency band (0.1 ~ 10 THz) can provide ultra-high transmitting rates for massive emerging applications. However, due to the radio frequency impairments and limited signal processing property of baseband devices, it is difficult for the current terahertz communication systems to be used in real applications. In this work, we report a 0.22 THz communication system, which can provide 84 Gbps air interface rate over 1.26 kilometers distance. Such a system is underpinned by three breakthroughs, namely, integrating the reported terahertz wireless communication system, redesigning the signal processing in baseband devices, and increasing the cut-off frequency and transmitting power of radio frequency component by parameter optimizing. Being applied to realize the real-time transmission of the uncompressed 8K ultra high-definition video in the 31st International University Sports Federation in Chengdu, China, this work is a leaping advancement to enable terahertz systems from experiment to promising applications.

Although millimeter wave (mmWave) (20 GHz–100 GHz) communications have been adopted to provide tens of gigabit per second (Gbps) transmitting rate in 5th generation mobile communication technology (5G)[1,2], there will be a huge gap to meet the rapid growth of the transmitting data in the future by 2030 and beyond, where the required transmitting rate would be hundreds of Gbps or even terabit per second (Tbps). By providing such high transmitting rate, terahertz (THz) communication systems operating between 100 GHz and 10 THz are promising to satisfy the explosive growth requiring transmitting ultra-fast for the emerging 6G and beyond applications, e.g., remote education (tens of Gbps), teleoperation (hundreds of Gbps), high-quality video conference (tens of Gbps), augmented reality (AR)/ virtual reality (VR) (hundreds of Gbps to tera bps), etc[3,4]. For instance, to achieve medical teleoperation assisted by AR/VR, the wireless transmission should be extremely reliable to guarantee the environment recovery without any error in AR/VR. In such teleoperation scenarios,

the 8K ultra high-definition (UHD) live video should be transmitted in real-time successfully for ultra-high resolution of the teleoperation[5].

Another typical application is the broadcasting of sports events[6] as shown in Fig. 1. This figure is a conceptual diagram of uncompressed UHD video transmission in sports event broadcasting based on THz wireless communication system in the future. The 8K UHD live video should be transmitted without compressing to guarantee the real-time requirement for the customers' immersive experience. Since the 8K UHD video is uncompressed, the content should be error-free at the receiver (Rx) for high-resolution environment reconstruction in VR/AR or display on the screen of the TV in live sports broadcast. By providing such high air interface rates, more redundancy can be transmitted via forward error correction (FEC) coding/decoding to guarantee both high signal rate and low error probability after decoding at the Rx. On the other hand, the narrow beamwidth of THz leads to a high received power at the Rx to enhance the reliability[3]. Thus, such applications can

[1]the National Key Laboratory of Wireless Communications, University of Electronic Science and Technology of China (UESTC), Chengdu, China. [2]School of Electronic Science and Engineering, University of Electronic Science and Technology of China (UESTC), Chengdu, China. [3]Terahertz Wireless Communications (TWC) Laboratory and the Department of Electronic Engineering and Cooperative Medianet Innovation Center (CMIC), Shanghai Jiao Tong University, Shanghai, China. [4]These authors contributed equally: Yinian Feng, Chong Han, Bo Chang, Zhi Chen. ✉e-mail: fengyinian@uestc.edu.cn; chong.han@sjtu.edu.cn; chenzhi@uestc.edu.cn; zhangbouestc@yeah.net
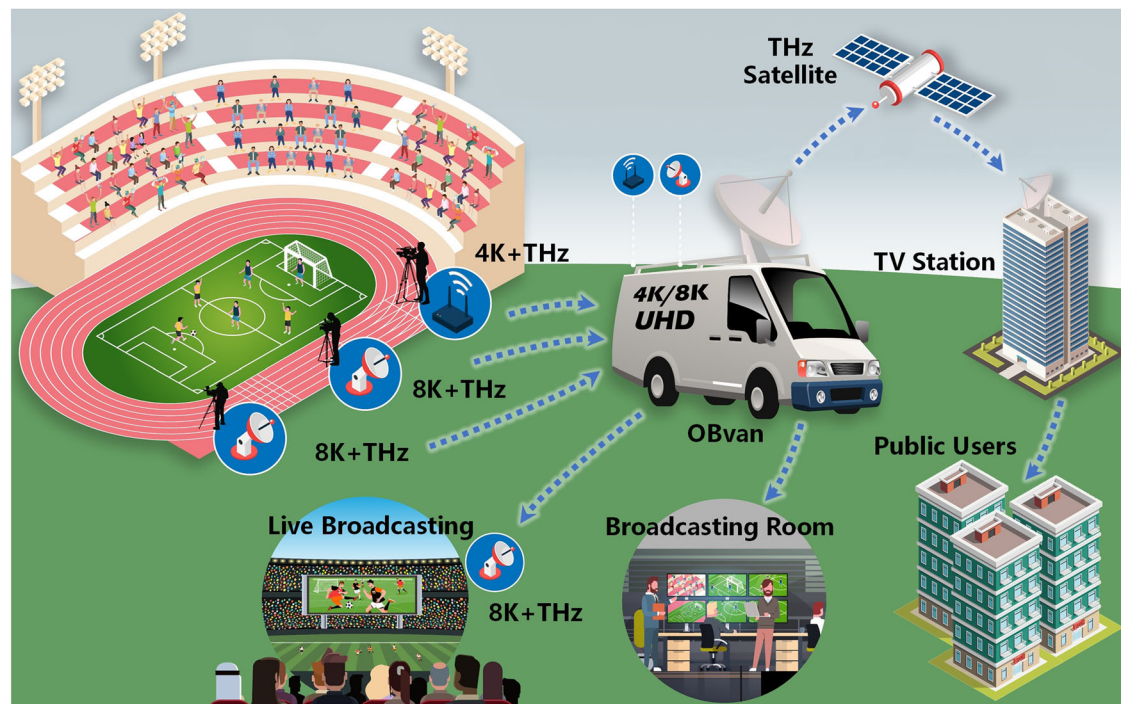
Fig. 1 | A conceptual diagram of UHD video transmission in sports event broadcasting based on THz wireless communication system in the future. Including 4K and 8K cameras, THz transmitters, outside broadcast van (OBvan) with THz receivers, THz satellites. 8K and 4K cameras send UHD live video of sports events via the THz wireless communication system to an OBvan. Then, OBvan casts the video to the screen in the competition site, and meanwhile sends the video to the broadcast room, where the video would be transmitted to the television (TV) station via THz satellite for further presentation to public audiences.

be fully supported by THz communication systems since they can provide hundreds of Gbps or even Tbps transmitting rate with high reliability[7].

However, the current THz communication systems (e.g., the systems in Refs. [8–24]) cannot be used in the aforementioned commercial applications because of the following three critical bottlenecks. The first one is the integration of the real-time THz wireless communication system. Since few works have been done on the application of the THz wireless control system in real world, the integration is an extremely challenging open problem. For instance, due to the aforementioned two bottlenecks, the interface between different modules should be carefully designed in the system integration to guarantee the real-time requirement. More importantly, the optimal system framework for real-world application is still an open problem, which determines the resource cost and performance of the whole system.

The second one is the limited signal processing property in baseband device. Most wireless communication prototypes adopt field programmable gate array (FPGA) as their signal processing device in baseband. Dealing with such high transmission rate via baseband is challenging in real-time, the ultra-high speed baseband signal processing in the existing THz communication systems is mainly offline. In other word, the Rx in the THz communication systems obtain the sent signal from the transmitter (Tx) in real-time, and then process the baseband signal by computers. However, signal processing for uncompressed 8K video must be real-time to be used in the aforementioned real-world applications, e.g., AR/VR. Therefore, it is necessary to design low complexity baseband algorithms to coordinate good system performance and limited hardware resource.

The third one is the radio frequency (RF) impairments. In THz frequency band, the high spreading loss and molecular absorption would cause severe signal attenuation. Then, high antenna gain is essential to balance the link budget. Since THz band is between millimeter-wave and infrared band, the generation of signals on THz band with high transmitting power is challenging by both electronic

components and photonic components, which would result in severe RF impairments, e.g., the imbalance between in-phase/quadrature (IQ) branches, non-linearity of power amplifier (PA), and the phase noise of local oscillator (LO).

We notice that some researches have been done on real-time signal processing in THz communication systems[17,25–31]. For instance, in Ref. [25], the authors achieved 1 Gbps transmitting rate with real-time signal processing by experiment. However, the data rate cannot support the uncompressed 8K video transmission. In addition, in[27], the authors developed a THz communication system with 0.3 THz to achieve the uncompressed 8K video transmission using OOK (On-Off Keying) modulation without bit error. However, the transmitting distance is about 2–3 cm, which cannot be used to support the aforementioned applications in real world. The main existing works on THz communication prototype with real-time signal processing are shown in Table 1. It is worth noting that due to the differences in hardware used and the complexity of digital signal processing, we only compare their core parameters. These values are only used for indication. In summary, all the existing works cannot be used for the real-time uncompressed 8K video transmission in real world because they do not satisfy the requirements.

In this work, we report a electronics-based 0.22 THz communication system by dealing with all the aforementioned challenges, which can provide 84 Gbps air interface rate at 1.26 kilometers (km) distance. We first develop the THz communication system for the real-time ultra-high transmission, which is based on the integration of the existing standardized commercial components, the proposed RF components, specific signal processing algorithms, and specific interfaces among different components and devices. Second, we redesign a baseband subsystem based on 16QAM-OFDM to achieve the high-throughput physical layer link for the ultra-high transmitting rate. A low complexity adaptive channel equalization algorithm is proposed to deal with the IQ imbalance problem. Finally, we cope with the problem in RF design to increase the transmitting power, reduce the

Table 1 | Comparsion of the main existing THz wireless transmission systems with real-time signal processing

Frequency band	Architecture	Distance(meter)	Bit rate(Gbps)	BER	Emitted power(dBm)	Modulation
400 GHz[25]	Photonics-based	35	1	1e-9	10	ASK
300 GHz[26]	Photonics-based	100	50	9.5e-4	−13	OOK
300 GHz[27,28]	Photonics-based	0.02– 0.03	48	1e-11	−15	OOK
220 GHz[17]	Electronics-based	1030	20.8	3.8e-7	−11.9 / −13.5 (two-channel)	16QAM
340 GHz[29]	Electronics-based	50	3	1.784e-10	17.5	16QAM
140 GHz[30]	Electronics-based	1500	2	1.80e-11	5	16QAM
300 GHz[31]	Electronics-based	10	1.68	/	/	16QAM-OFDM
This work	**Electronics-based**	**1260**	**84**	**1e-15/0**[*]	**9.7/10.3 (two-channel)**	**16QAM-OFDM**

0 BER indicates there is no bit error within the first two hours of continuous observation, which has the same meaning in the rest of this paper

[*]1e-15 BER in this work indicates the bit error within six hours of continuous observation.
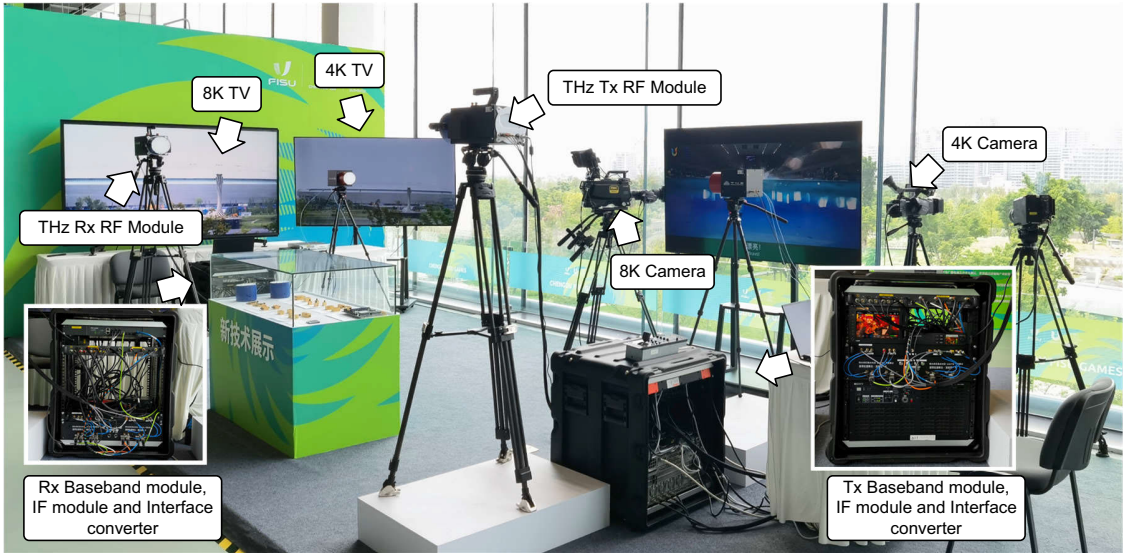
Fig. 2 | The THz system exhibited at the Main Media Center of the 31st International University Sports Federation (FISU) in Chengdu. The exhibition presents the overall system and the components for the system. Meanwhile, a 4K video is presented for comparison to highlight the video quality and visual experience of the 8K video.

non-linearity domain of PA and phase noise of LO, and suppress the imbalance between IQ branches. By providing 84 Gbps air interface transmitting rate, the reported THz wireless communication system has been used to support the real-time transmission of the uncompressed 8K UHD video in the 31st International University Sports Federation (FISU) in Chengdu, China. Outdoor experiments of this system and the application in FISU are shown in Supplementary Video 1. By such an application, the potential usage of the proposed system in real world has been verified, we believe this is a critical step to enable terahertz systems from experimental to commercial applications.

Results
The adopted THz wireless system in FISU and the performance
Recall Fig. 1, the reported THz wireless communication system has achieved the uncompressed 4K and 8K UHD video transmission from the camera to the OBvan in FISU in Chengdu, China. The adopted THz wireless system exhibited in the main media center of FISU in Chengdu is shown in Fig. 2. The overall architecture of this system is shown in Fig. 3a. The developed system was responsible for 8K video transmission. The real-time video captured by the 8K camera is the input data source, which is operated by the camera control unit (CCU), and then sent to the baseband platform through optical fiber in the form of high-speed data stream based on serial digital interface (SDI) protocol[32]. After signal processing in baseband module and intermediate frequency (IF) module, the encoded and modulated signal

would be transmitted by THz RF module in Tx. Then, the signal would be received by THz Rx RF module. Finally, the video is converted into high definition multimedia interface (HDMI) format and displayed on 8K TV screen after demodulating and decoding.

The integration of the hardware architecture of the THz wireless communication system is shown in Fig. 3b. The 8K video data stream is divided into four 4K video streams, which are left top (LT), right top (RT), left bottom (LB), and right bottom (RB). After the dividing, the baseband receives the video data in SDI format. The baseband signal processing of both Tx and Rx is operated by two high-performance FPGAs, respectively. Each FPGA conducts the signals of two channels consisting of 4K video streams. Dual digital to analog converters (DACs) are adopted for each 4K video stream at the Tx to product in-phase (I) and quadrature (Q) branches. Meanwhile, dual analog to digital converters (ADCs) are adopted for each 4K video stream at the Rx to receive I and Q branches. At the Tx, the analog signal output by DACs is sent to the IQ mixer with 9 GHz as the IF LO. Then, the IF signal within 6.3 GHz–11.7 GHz is mixed to the THz frequency band via harmonics by the THz mixer, which is conducted by adopting the second harmonic produced by doubling the frequency of the LO signal. The THz LO is generated by RF LO1 ~ 4 in RF module as shown in Fig. 3c, where the generated four THz LO are 212.8 GHz, 218.4 GHz, 207.2 GHz and 212.8 GHz, respectively. The total bandwidth of the THz wireless communication system is 5.25 GHz × 4 = 21 GHz. Noting that the data setting here are determined by the signal processing in baseband, which
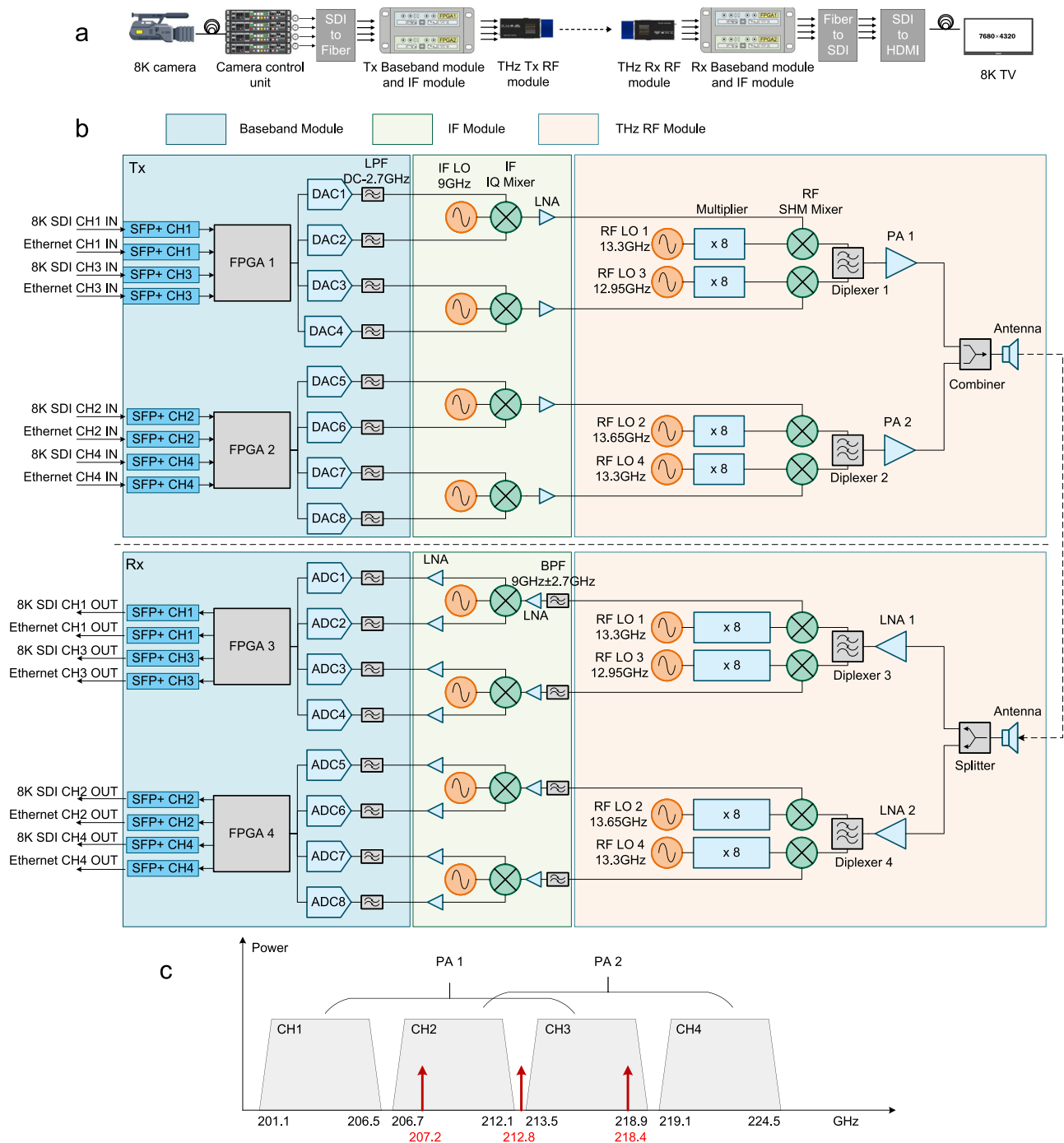
Fig. 3 | The architecture of the THz wireless communication system and spectrum usage. a The overall architecture of the system. **b** The integration of the hardware architecture of the system. The 8K video data stream is divided into four 4K video streams. The system mainly consists of FPGAs, analog to digital converters (ADCs), digital to analog converters (DACs), filters, local oscillators, IQ mixers, frequency multipliers, sub-harmonic mixers (SHMs), diplexers, power amplifier (PAs) and noise amplifierd (LNAs). The three shades in the figure represent Baseband Module, IF Module and THz RF Module from left to right. **c** THz band usage. The gray portions represent the frequency bands of the four channels, the red marks indicate the THz local frequency.

would be discussed in the next section. A diplexer is used for RF chain aggregation. In addition, the PAs are used to amplify the aggregated signal. Finally, the signal transmitting is carried out by a lens antenna. After receiving the signal, the Rx performs the reverse operation. Different from Tx, the RF chain is equipped with a low noise amplifier (LNA) with gain of 20 dB. In addition, a zero IF sampling method is adopted in this system, which can suppress the image interference and significantly increase the bandwidth of the baseband for each chain with limited ADC/DAC property.

Before using in FISU, the performance of the reported THz wireless system was first evaluated at 1.26 km distance between transceiver for error-free uncompressed 8K video transmission. The received power can be expressed as

$$P_r = P_t + G_t - L_f - L_{atm} + G_r \tag{1}$$

where P_t is transmitting power, G_t and G_r represent the gain of the transmitting and receiving antennas, respectively. In addition, L_f is the

Table 2 | The performance of the uncompressed 8K video real-time wireless transmission system

Parameter	Value	Parameter	Value
Air interface rate	84 Gbps	SNR	>18 dB
Service rate	63.52 Gbps	BER	0
Bandwidth	21 GHz	Distance	1260 m
System Delay	<50 μs	Modulation	16QAM-OFDM
Transmitting power	9.6 dBm/10.3 dBm	Antenna gain	55 dBi

path loss caused by free space attenuation, and L_{atm} indicates the attenuation caused by atmospheric loss. The path loss L_f can be calculated by

$$L_f = 92.4 + 20\lg f + 20\lg d \qquad (2)$$

where f indicates the operating frequency and d is the transmission distance, we can get L_f is 140.85 dB when f is 210 GHz and d is 1.26 km. The environmental condition is as follows: 36 temperature, 70% humidity, and 29.16 g/m³ corresponding water vapor density. According to ITU-R[33], we can get L_{atm} as 16.13 dB. When the transmitting power is 10 dBm and the antenna gain of the transceiver is 55 dBi, the received power is estimated to be −37.0 dBm according to equation (1). In the experiment, the output power of PA1 and PA2 are 9.6 dBm and 10.3 dBm, respectively. Cassegrain antennas with a diameter of 45 cm and a gain of 55 dBi are used. The system achieves error-free uncompressed 8K video real-time transmission at 1.26 km. The video on the 8K TV is smooth without fragmentation, which means that the baseband signal processing and RF channels can maintain good delay consistency. By measuring the receiving power of the IF signal, the received power of the THz antenna can be calculated, which is about −38.20 dBm. Furthermore, the power consumption is measured as 199 W at the Tx and 226.04 W at the Rx, respectively, in which the RF front end power is about 60 W. Compared with the specific base station (BS) with 4-port MIMO in 5G (the power consumption of the RF is about 4 × 40 W, and meanwhile the total power consumption of the BS is about 1060 W)[34], the power consumption is acceptable as a prototype. With the growing development of THz components and systems, the power consumption is expected further reduced to satisfy the commercial applications. Compared with the chipset in commercial E-bands, the power consumption of the baseband signal processing in FPGA is higher and can reach to about 70 W. On the other hand, the RF front end is designed for high transmitting rate with long distance. Meanwhile, due to the limited of the current foundry technology for the THz components, the energy efficiency is not high enough for commercial applications, which is expected to be solved with the development of the foundry technology. Higher than the RF front end in commercial E-bands, the power consumption of the RF front end in the THz system reaches 129 W. In terms of the THz system including the RF front end, the overall power consumption is 199 W in our THz Tx. Since the air interface rate is 84 Gbps, the energy per bit equals to 2.3 nJ/bit, which is close to that in commercial devices with E-bands, i.e., 2.3 nJ/bit in[35]. We clarify that only physical layer is considered in the THz system, while both physical layer and upper layers are considered in commercial E-bands, which would influence the results of energy efficiency. We could reasonably anticipate that the energy per bit performance can be significantly improved for future commercial THz systems, where the signal processing is expected to be operated on chipset, the foundry technology is expected to guarantee the specific applications, and the RF front end is expected to be produced with small size and low energy consumption. Thus, the commercial usage of THz communication systems is promising. The system performance with 1.26 km is summarized in Table 2.

Figure 4a illustrates the deployment of the THz wireless system in the track and field events of FISU in Chengdu. As shown in this figure, due to area restrictions, the Txs are located at three independent points, each of which is responsible for a specific area. Rx is placed across the field on the other side, where the broadcasting room and OBvan can process the video sent from the Rx via fiber. The distances between transceiver are 87 m, 153 m, and 180 m, respectively. The distance 180 m between transceiver is adopted to show the performance of the reported system in FISU, where the output power of PA1 and PA2 is reduced to 0.31 dBm and 0.20 dBm by attenuators decreasing the output power of the IF module, respectively. Furthermore, a smaller lens antennas with a diameter of 15 cm and a gain of 44 dBi is adopted to minimize the size of the THz system for mobility. The received power of THz antenna is −38.72 dBm, which is similar to that in the test with 1.26 km and means that the error-free uncompressed 8K video transmission can be achieved. A spectrograph is used to collect test data for performance evaluation. The spectrums and constellations of the four video stream channels are shown in Fig. 4b and c, respectively, which indicates that the data can be successfully recovered at the Rx. Meanwhile, we summarize the corresponding signal-to-noise-ratio (SNR), bit-error-rate (BER), and error vector magnitude (EVM) of the four video streams at the Rx in Table 3, we can conclude that the BER of this system is 0, which can support the uncompressed 8K UHD video transmission with ultra-high reliability. Note that the BER of the adopted QAM modulation can be calculated by $\text{BER} = 4 \cdot \left(\sqrt{M}-1\right)/\sqrt{M}Q\left(\sqrt{3\log_2(M)\cdot \text{SNR}/(M-1)}\right)$[36], where $Q(\cdot)$ represents Q-function and M is the order of the QAM modulation. In addition, a (255,226) Reed-solomon (RS) code with an encoding efficiency of 88% is adopted in this article, which can provide another 5 dB encoding gain and would be discussed in detail in the next subsection. In FISU experiment, the measured SNR at the receiver is about 18.46–19.48 dB, which leads that the corresponding BER is 2.973×10^{-27} ~ 1.840×10^{-34}. To this end, the observed BER of the experimental system is 0. This is explained that there is no bit error occurred within two hours of continuous observation. Related to video streaming, there are no bad spots, black screens and out-of-sync situations on the TV. More details about the BER can be found in the Supplementary Discussion 1. Such a BER performance was reported in Ref. 20.

Baseband design and real-time signal processing

The wireless transmission for uncompressed 8K video requires a traffic rate of 48 Gbps to guarantee the real-time requirement. In addition, there is an urgent need for strict frame synchronization and ultra-low bit error rate to support the uncompressed 8K video transmission. This lays challenges on baseband design and implementation in the THz wireless system deployment. To overcome the wireless channel gain between transceiver and achieve ultra-high reliability, appropriate baseband algorithms design and data redundancy are required. Furthermore, in order to implement real-time digital signal processing (DSP) on FPGA, effective strategies must be developed to reduce the usage of resources and ensure that clock constraints are satisfied. To maintain the above requirements, 16 quadrature amplitude modulation and orthogonal frequency division multiplexing (16QAM-OFDM) communication framework is adopted in the reported system. The reasons adopting OFDM are as following.

1. OFDM allows the carrier spectrum to overlap with each other. Compared with signal carrier frequency, the spectrum utilization in OFDM is significantly improved due to the orthogonality between the sub-channels, where the bandwidth can be sufficiently used and the consumption of hardware resource can be significantly reduced.

2. Since the system uses zero-IF construct is adopted for data transmission, the direct current (DC) component caused by the local vibration leakage problem will inevitably introduce
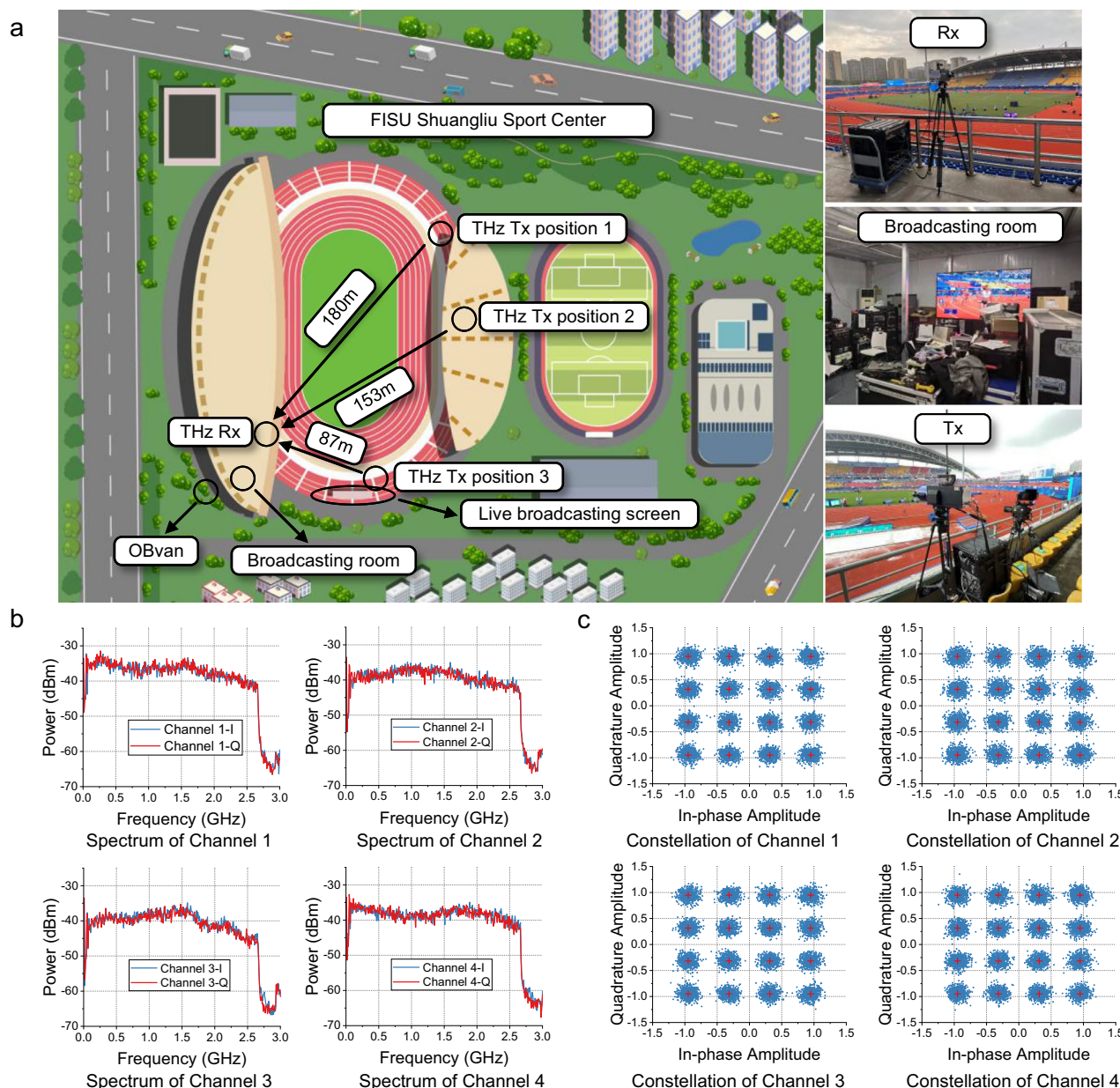
Fig. 4 | Field deployment and test results. a Location information of each component of the stadium. There are three Txs located at different positions, each of which is responsible for a specific area, Rx is placed across the field on the other side. **b** Accepted spectrum for each 4K video streaming channel. **c** Constellation maps for each 4K video streaming channel. Source data of (**b**) and (**c**) is provided as a Source Data file and named as "Fig. 4-b" and "Fig. 4-c".

interference with the baseband signal. In addition, in RF links, the linearity of the device to the high-frequency part of the signal bandwidth is worse than that of the low-frequency part. Then, we can flexibly choose subcarriers to suppress these interferences.

3. The frequency response caused by the RF front end can be suppressed by OFDM waveform design, and meanwhile the intersymbol interference can be solved by introducing applicable cyclic prefix (CP) in OFDM waveform design.

Table 3 | SNR, BER and EVM of the four video stream channels

Channel	SNR	EVM	BER before Decoding	BER after Decoding
1	19.48 dB	7.92%	8e-7	0
2	18.46 dB	9.52%	1.1e-6	0
3	19.24 dB	8.37%	1.2e-6	0
4	19.12 dB	8.52%	9e-7	0

To ensure ultra-low error rate in the video transmission in case of the fluctuation of receiving power or signal-to-noise ratio (SNR), a (255,226) RS code is designed with an encoding efficiency of 88%, where more 5dB encoding gain can be provided. Since the statical point-to-point (P2P) THz wireless communication is adopted in this article, burst error dominate the transmitting error of the system, which is another important reason to adopt RS code since it is the best choice to deal with the burst error.

The design of the subcarriers, the frame structure, and the baseband signal processing flow can be found in Supplementary Fig. 9. For frame synchronization, a combination of coarse synchronization and fine synchronization is adopted, where the computing complexity can be significantly reduced compared with the traditional frame synchronization with matched filtering method[37]. Considering the consumption of synchronization frame and training frame, the maximum service rate of baseband can be 15.88 Gbps.

In this system, the two IQ signals are transmitted independently by two channels to support the ultra-high transmission rate, the difference of simulator parts and manufacturing process defects cause the imbalance of IQ signal in amplitude and phase. The IQ imbalance will affect the maximum transmission distance and signal quality of the system, or even result in the failure of the frequency offset correction algorithm. Especially in high-frequency systems with high order modulation, the negative effect of IQ imbalance would be even worse[38]. In conventional methods, the IQ correction and channel correction are conducted separately. Such methods cannot be used in our proposed system since a lot of hardware resource is provided for ultra-high data processing and the left limited resource cannot support the separate conduction[39]. To deal with this issue, we propose a novel adaptive IQ and channel correction method with low-complexity in frequency domain based on least mean square (LMS), where the imbalance of IQ, channel, phase, and frequency can be solved simultaneously. The signal intended to be transmitted at Tx can be expressed as:

$$\mathbf{s}(t) = \mathbf{s}_i(t) + \mathbf{s}_q(t). \tag{3}$$

The received signal by Rx can be expressed as:

$$\mathbf{r}(t) = \mathbf{g}_1(t) \otimes \mathbf{s}(t) + \mathbf{g}_2(t) \otimes \mathbf{s}^*(t) + \mathbf{w}(t), \tag{4}$$

where $\mathbf{g}_1(t)$ and $\mathbf{g}_2(t)$ are the joint impulse response consisting of the IQ imbalance at Tx, the IQ imbalance at Rx, and the impulse response of the channel. Since the P2P static communication is adopted, the Doppler shift can be ignored. Then, the error function can be expressed as

$$\mathbf{E}(k) = \mathbf{Y}(k) - \mathbf{S}(k) = \mathbf{Y}(k) - \mathbf{X}(k)^\mathrm{T}\mathbf{W}(k), \tag{5}$$

where $\mathbf{S}(k)$ indicates the output balanced signal of the current k-th OFDM symbol subcarrier. According to the minimum variance criterion, this problem can be converted into an optimization problem, i.e., minimizing the following objective function:

$$\mathrm{J}_{\mathrm{LMS}}(\mathbf{W}) = \mathrm{E}\{|\mathbf{E}(k)|^2\} = \mathrm{E}\{|\mathbf{Y}(k) - \mathbf{X}^\mathrm{T}(k)\mathbf{W}(k)|^2\}. \tag{6}$$

When the weight coefficient $\mathbf{W}(k)$ iterates following the negative gradient direction, the weight coefficient of the next $(k + 1)$-th OFDM symbol subcarrier can be expressed as

$$\mathbf{W}(k + 1) = \mathbf{W}(k) + \lambda\mathbf{E}(k)\mathbf{X}^*(k), \tag{7}$$

where λ is the iteration step. The LMS algorithm in frequency domain is used to estimate the frequency-domain response of each subcarrier to compensate the effect caused by the imbalance of both channel and IQ, where the requirements of high-speed data processing can be maintained and meanwhile the resource consumption can be significantly reduced.

The delay performance of baseband loopback is shown in Fig. 5. We collect both the video SDI data obtained in the baseband of the Tx and the received video SDI data in the baseband of the Rx by an oscilloscope. Then, the autocorrelation of them is adopted to obtain the delay of the basedband loopback. From the figure, the delay of baseband loopback is 48.9048 μs, where the delay over the cable can be negligible. For the whole system, the transmission delay of the signal in the RF link and media is nanosecond level. Thus, we can obtain that the overall delay of this system will not exceed 50 μs, which means that real-time property can be guaranteed by the proposed system.
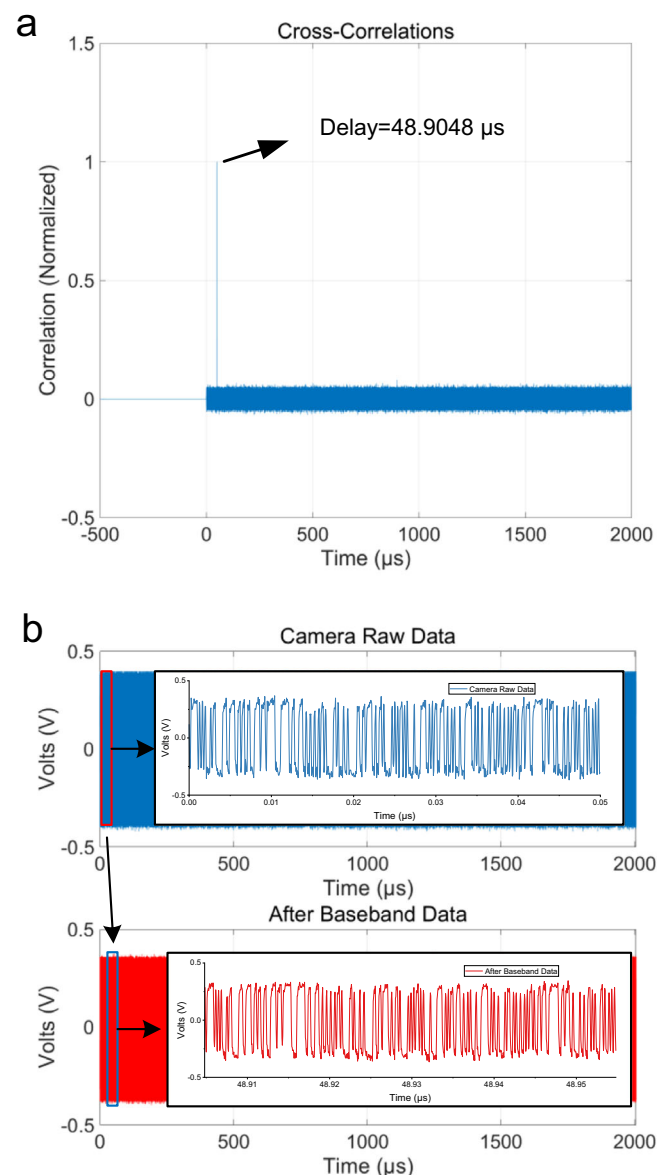
Fig. 5 | Time delay of the loopback in baseband. a Autocorrelation values for time delay calculation. **b** Waveform for time delay calculation.

RF chain and key components for the THz wireless system

The RF chain is responsible for the modulating and transmitting analog signal between DACs/ADCs and THz frequency band. A double-layer and symmetrical structure is adopted for high integration. The core components include 220-GHz sub-harmonic mixers (SHMs), 220-GHz diplexers, PAs, LNAs and lens antennas. The layouts of the RF module at Tx and Rx are shown in Fig. 6. The 220-GHz SHM has been developed to generate and detect carrier signals, which is based on antiparallel Schottky barrier diodes (SBDs)[17]. To satisfy the design requirements of the 220-GHz SHM, a 3-D electromagnetic (EM) peripheral structure model are adopted to build the model of SBDs. By the distributed extraction method of diode embedded impedance, the optimal impedance matching conditions can be extracted by adjusting the source and load impedance at both ends of diodes. Based on the harmonic balance (HB) simulation method, when the LO frequency and RF are set to 105 GHz and 220 GHz, the driving and input power are set to 2 mW and -30 dBm, respectively, the optimal conversion loss of the SHM is calculated as 5.5 dB. The 220 GHz SHM is developed based on the quartz substrate of 50 μm thickness. The RF and LO signals are
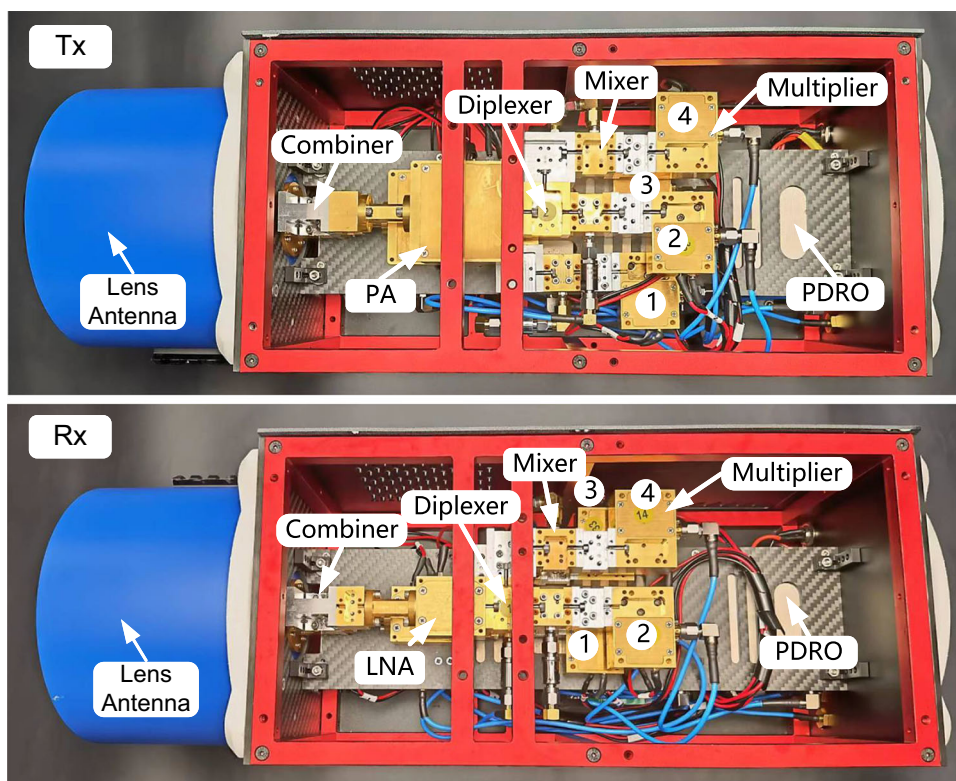
Fig. 6 | The layout of the RF module at Tx and Rx. Double-layer and symmetrical structure is adopted for high integration. The numbers 1–4 indicate the four channel.

input through the WR-4.3 band and WR-8 band standard waveguides, respectively. By waveguide-microstrip transition structure, the TE_{10} mode of waveguide is converted to quasi-TEM mode of suspended microstrip. Photographs of the designed SHM are shown in Fig. 7a and b. The split blocks of the SHM were fabricated by computer numerical control (CNC) milling. The Schottky diode is flip-chip mounted on the quartz substrate. By fixing the LO frequency as 207.2 GHz, 212.8 GHz and 218.4 GHz and changing RF frequency, the conversion loss of the proposed mixer is obtained by measured the IF output power. The measured results are shown in Fig. 7c, it can be seen that the conversion loss for four channels is less than 9 dB. More details are presented in Supplementary Method 1.

The 220-GHz diplexer is mainly used to aggregate and separate two carrier signals and meanwhile filter the side band signal that is not needed in the mixer. In order to solve the problem of poor suppression effect of traditional Chebyshev filter in high stopband, two singlet-based quasi-elliptic filters are designed for channel filters[40]. In this work, two kinds of singlet, which are based on the coupling of TE_{301} and TE_{102} modes and TE_{201} and TE_{101} modes, respectively, are used in the design of the 220 GHz diplexer. Details of the design and optimisation of the singlet-based quasi-elliptic filter are presented in Supplementary Method 2. To ensure the sufficient isolation among each channel, diplexer 1 and 2 are composed of channel 1&3 and 2&4, respectively, channel 1 and 2 filters are designed as fifth-order, while channel 3 and 4 filters are fourth-order. Based on the aforementioned channel filters, the proposed diplexer is developed using T-junction, which as shown in Fig. 7d. Two channel filters are connected directly to the T-junction via waveguide transmission lines of l_{s1} and l_{s2}, where the initial values of l_{s1} and l_{s2} are set as half of waveguide wavelength ($\lambda_g/2$) at the center frequency of the corresponding channel. The proposed diplexers are fabricated by CNC milling, which are shown in Fig. 7e and f. Two split blocks of diplexer are aligned by inner pins under the microscope for alignment accuracy. The measured results are shown in Fig. 7g, where the channel isolation of the diplexer can reach more

than 50 dB, and meanwhile the insertion loss is less than 2 dB. In summary, the two diplexers have good frequency response characteristics in the corresponding operating frequency. In addition, the interference between the four channels can be well isolated by the IF down-conversion and bandpass filtering at the Rx. The suppression of LO signals of the aforementioned diplexer is more than 45 dB, which can prevent LO signals from leaking into the subsequent power amplifier resulting in reduced output power of PA. This is an important reason for the reported system to achieve both long-distance transmission and ultra-high transmitting rate.

The adopted PAs and LNAs are produced by our partners and customized for the THz systems. Figure 7h shows the photograph of the adopted PAs. PA1 is used to amplify the aggregated signals from channel 1 and channel 3. PA2 is used to amplify the aggregated signals from channel 2 and channel 4. A THz vector network analyzer is used to measure the gain of the two PAs, where the measured gain is shown in Fig. 7i. From Fig. 7j, the measured saturated output power exceeds 20 dBm at 0.22 THz. Furthermore, LNA1 and LNA2 are corresponding to channel 1/channel 3 and channel 2/channel 4 at the Rx, which is shown in Fig. 7k. The gain of two LNAs is also measured by THz vector network analyzer, which is shown in Fig. 7l. Besides, the measured noise figure of the four channels is shown in Fig. 7m, which are all strictly less than 8 dB. In this work, the performance of above modules can guarantee the system requirements.

Discussion

Compared with the existing THz communication systems, we focus on the real world application of the THz wireless communication system, where a real-time THz wireless communication system is built by integrating the existing commercial components (e.g., FPGA and ADC/DAC), low complexity baseband algorithm, and new designed RF components. This system is implemented for the real-time transmission of the live uncompressed 8K video in FISU in Chengdu, China. We discussed the proposed system in details from
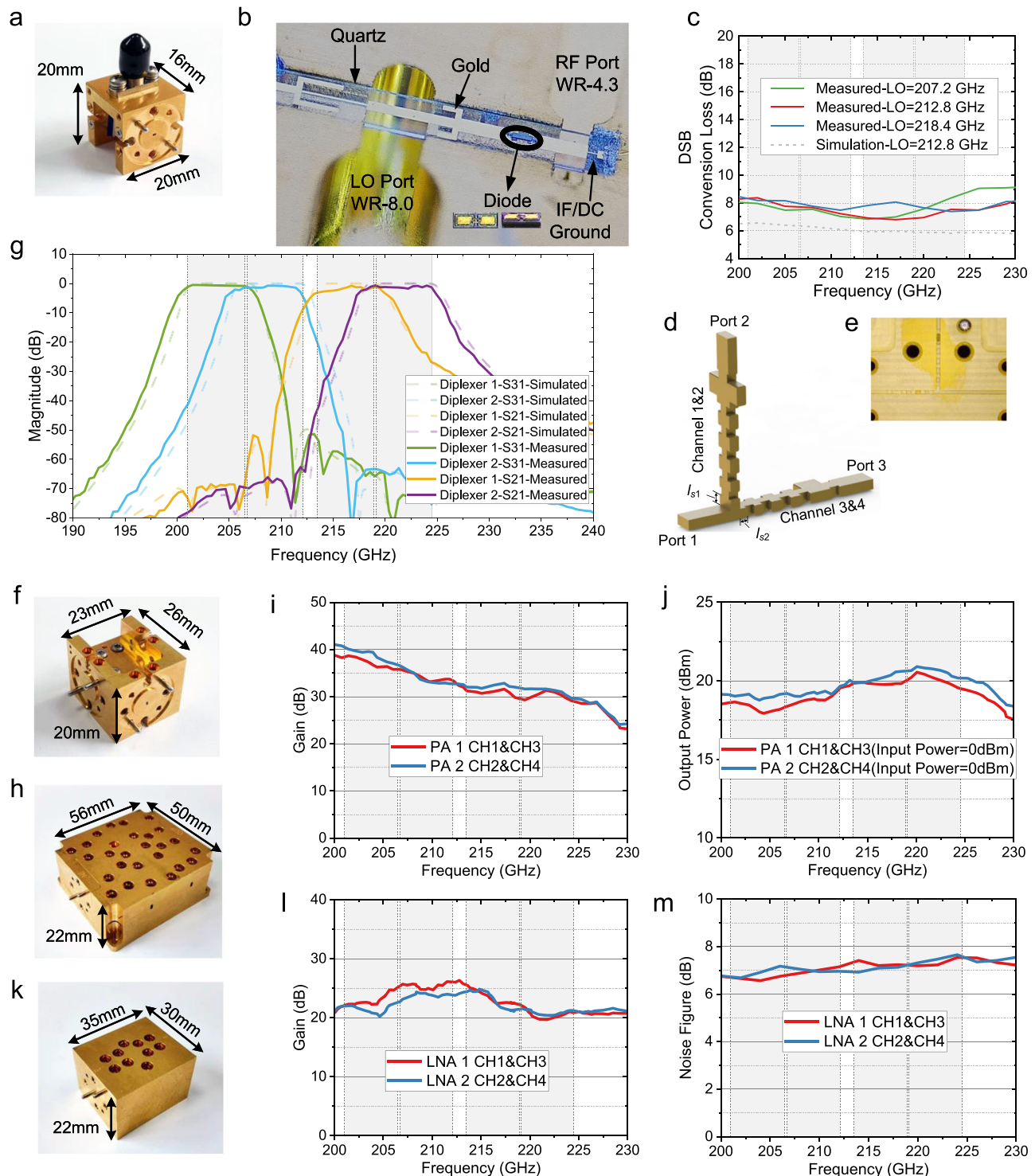
Fig. 7 | The 220-GHz SHMs, the 220-GHz diplexers, PAs and LNAs used in the system. a The photograph of the 220-GHz SHM. **b** Internal structure of the 220-GHz SHM. **c** Measured results of the 220-GHz SHM. **d** The structure of the 220-GHz diplexer. The proposed diplexer is developed using T-junction. **e** Internal structure of the 220-GHz diplexer. **f** The photograph of the 220-GHz diplexer. **g** Measured results of the diplexers. **h** The photograph of the PAs. **i** Measured gain of the PAs. **j** Measured output power of the PAs. **k** The photograph of the LNAs. **l** Measured gain of the LNAs. **m** Measured noise figure of the LNAs. The gray portions in (**c**), (**g**), (**i**), (**j**), (**l**), (**m**) represent the frequency bands of the four channels. Source data of (**c**), (**g**), (**i**), (**j**), (**l**), (**m**) is provided as a Source Data file and named as "Fig. 7-c", "Fig. 7-g", "Fig. 7-i", "Fig. 7-j", "Fig. 7-l", "Fig. 7-m".

design guidelines to practical implementation. The results collected at FISU shown that the achieved air interface rata is 84 Gbps with 16QAM-OFDM modulation. In addition, the transmission time delay is less than 48.9048 μ s. Furthermore, the BER is zero within two hours of continuous observation time, which can guarantee the ultra-reliable requirement. Then, the proposed system can successfully support the live uncompressed 8K video transmission at a distance of 1260 m. We believe this is a critical step to enable terahertz systems from experimental to commercial applications.

Since each channel of the 8K camera uses only 12 Gbps data rate, the maximum service rate of the designed baseband is 15.88 Gbps to maintain the required data rate. We further designed a 10GBASE-R Ethernet interface for sending one-way Ethernet data streams based on UDP protocol from Tx to Rx. The Ethernet ports of these four channels are aggregated to achieve an end-to-end data rate of 12 Gbps. Then, multiple 4K/8K compressed video streams can also be transmitted by the proposed system. By dividing each 4K 60 frame uncompressed camera signal (12G-SDI) into four 3G SDI signals to access the system, the system can simultaneously support the transmission of each uncompressed 4K 60 frame and each uncompressed 8K 60 frame camera signal. This is verified in Figs. 3b and 5c.

Compared with single-carrier communication systems, the PAPR problem is challenging in OFDM systems. When the peak signal enters the nonlinear region of DACs and high-power amplifiers (HPAs), in-band distortion and out-of-band radiation would be generated. Then, signal distortion or adjacent frequency interference would be introduced. The power efficiency would be significantly reduced, which further results in the deterioration of system performance, especially in THz communication systems. In the reported THz wireless communication system, a careful designed ZC sequence in synchronization processing is adopted to deal with PAPR. The research of low-complexity algorithms based on probability theory may be a promising direction, which is also a topic for the team to continue to study.

It is also worth to note that a small-caliber antenna is chosen for the uncompressed 8K video THz communication system to achieve the transmission for FISU, where the integration, miniaturization, and portability are fully considered to further support the mobility of the system. At the same time, considering the outdoor weather conditions during FISU, the ability to prevent rain and heat dissipation is considered.

Methods

The calculation of the BER

RS code is also named as (n,k) code, where n is the total number of symbols in the code block and k is the number of information or data symbols. The code block consists of k data symbols and $(n - k)$ check symbols. RS code is a typical forward error correction code (FEC). After decoding calculation and verification, we can obtain the number of error bits and the total number of bits after decoding. By AXI4-Stream bus protocol, we can read the valid status information of RS decoding module at the Rx. In the reported system, the number of error bits and the total number of bits in 16 parallel RS decoding modules are sent to the computer via UDP protocol and Ethernet interface at a frequency of about 18 Hz for BER calculation, where the length of the data before RS decoding for each calculation is 1.0974×10^9 bits. In addition, the channel state information (CSI) of the four wireless channels are also uploaded for system parameter adjustment to achieve the required transmission performance.

The 220-GHz SHM and the 220-GHz diplexer

The 220-GHz SHM is developed based on the quartz substrate of $50\,\mu$m thickness, where the structure is shown in supplementary Fig. 1. In this work, a planar antiparallel Schottky diodes chip is adopted, the Schottky diode is flip-chip mounted on the quartz substrate. The 3-D EM model of Schottky diode chip can be seen in supplementary Fig. 2. More information about the parameters of the SHM and the optimal embedding impedance of the SHM can be found in Supplementary method 1. The 220-GHz diplexer is designed and fabricated based on the quasi-elliptical filter, where two kinds of singlet, based on the coupling of TE_{301} and TE_{102} modes and TE_{201} and TE_{101} modes as shown in supplementary Fig. 4 and supplementary Fig. 5, are adopted to improve the isolation between channels. More design details and simulation results about diplexer and channel filters can be found in Supplementary method 2.

Data availability

Source data are provided with this paper.

Code availability

All codes are integrated into the system framework, which is delivered to the Technique and Service Department of Chengdu Radio and Television Station. A Cooperative Research and Development Agreement or memorandum of understanding is needed between the requester's organization, the authors' organization, and the Department to obtain these codes. To obtain such an agreement, please contact the corresponding author, who will guide the requester through the necessary steps.

References

1. Xiao, M. et al. Millimeter wave communications for future mobile networks. *IEEE J. Selected Areas Commun.* **35**, 1909–1935 (2017).
2. Jia, S. et al. Integrated dual-laser photonic chip for high-purity carrier generation enabling ultrafast terahertz wireless communications. *Nat. Commun.* **13**, 1388 (2022).
3. Chen, Z. et al. A survey on terahertz communications. *China Commun.* **16**, 1–35 (2019).
4. Sarieddeen, H., Alouini, M. S. & Al-Naffouri, T. Y. An overview of signal processing techniques for terahertz communications. *Proc. IEEE* **109**, 1628–1665 (2021).
5. Mochida, Y., Shirai, D. & Takasugi, K. Ultra-low latency 8K video-transmission system utilizing disaggregation configuration. in *2022 IEEE Symposium in Low-Power and High-Speed Chips (COOL CHIPS, 2022),* 1-3 (Tokyo, 2022).
6. Kosugi, T., Hirata, A., Nagatsuma, T. & Kado, Y. MM-wave long-range wireless systems. *IEEE Micro. Mag.* **10**, 68–76 (2009).
7. Chaccour, C., Soorki, M., Saad, W., Bennis, M. & Popovski, P. Can terahertz provide high-rate reliable low-latency communications for wireless VR? *IEEE Int. Things J.* **9**, 9712–9729 (2022).
8. Nagatsuma, T., Ducournau, G. & Renaud, C. Advances in terahertz communications accelerated by photonics. *Nat. Photon.* **10**, 371–379 (2016).
9. Koenig, S. et al. Wireless sub-thz communication system with high data rate. *Nat. Photon.* **12**, 977–981 (2013).
10. Jia, S. et al. Integrated dual-DFB laser for 408 GHz carrier generation enabling 131 Gbit/s wireless transmission over 10.7 meters. in *2019 Optical Fiber Communications Conference and Exhibition (OFC, 2019),* 1-3 (San Diego, 2019).
11. Song, H., Hamada, H. & Yaita, M. Prototype of KIOSK data downloading system at 300 GHz: design, technical feasibility, and results. *IEEE Commun. Mag.* **56**, 130–136 (2018).
12. Zhang, J. et al. 6G oriented 100 GbE real-time demonstration of Fiber-THz-Fiber seamless communication enabled by photonics. in *2022 Optical Fiber Communications Conference and Exhibition (OFC 2022),* 1-3 (San Diego, 2022).
13. Koenig, S. et al. Wireless sub-THz communication system with high data rate enabled by RF photonics and active MMIC technology. in *2014 IEEE Photonics Conference,* 414-415 (San Diego, 2014).
14. Jia, S. et al. 0.4 THz photonic-wireless link with 106 Gb/s single channel bitrate. *J. Lightwave Technol.* **36**, 610–616 (2018).
15. Harter, T. et al. Generalized Kramers-Kronig receiver for coherent terahertz communications. *Nat. Photon.* **14**, 601–606 (2020).
16. Niu, Z. et al. The research on 220GHz multicarrier high-speed communication system. *China Commun.* **17**, 131–139 (2020).
17. Feng, Y. et al. A 20.8-Gbps dual-carrier wireless communication link in 220-GHz band. *China Commun.* **18**, 210–220 (2021).
18. Mehdi, I., Siles, J. V., Lee, C. & Schlecht, E. THz diode technology: status, prospects, and applications. *Proc. IEEE* **105**, 990–1007 (2017).
19. Wu, Q. et al. A 21km 5Gbps real time wireless communication system at 0.14 THz. in *2017 42nd International Conference on Infrared,*

Millimeter, and Terahertz Waves (IRMMW-THz, 2017), 1-2 (Cancun, 2017).

20. Sen, P., Siles, J. V., Thawdar, N. & Jornet, J. M. Multi-kilometre and multi-gigabit-per-second sub-terahertz communications for wireless backhaul applications. *Nat. Electron.* **6**, 164–175 (2023).

21. Hamada, H. et al. 300-GHz. 100-Gb/s InP-HEMT wireless transceiver using a 300-GHz fundamental mixer. in *2018 IEEE/MTT-S International Microwave Symposium (IMS, 2018)*, 1480-1483 (Philadelphia, 2018).

22. Lee, S. et al. An 80-Gb/s 300-GHz-band single-chip CMOS transceiver. *IEEE J. Solid-State Circuits* **54**, 3577–3588 (2019).

23. Hamada, H. et al. 300-GHz-band 120-Gb/s wireless front-end based on InP-HEMT PAs and mixers. *J. Solid-State Circ.* **55**, 2316–2335 (2020).

24. Jyo, T. et al. 220-to-320-GHz fundamental mixer in 60-nm InP HEMT technology achieving 240-Gbps dual-band data transmission. *IEEE Trans. Micro. Theory and Tech.* **72**, 516–524 (2024).

25. Ma, J., Shrestha, R., Moeller, L. & Mittleman, D. M. Channel performance for indoor and outdoor terahertz wireless links. *APL Photon.* **3**, 051601 (2018).

26. Nagatsuma, T. et al. 300-GHz-band wireless transmission at 50 Gbit/s over 100 meters. in *2016 41st International Conference on Infrared, Millimeter, and Terahertz waves (IRMMW-THz, 2016)*, 1-2 (Copenhagen, 2016).

27. Webber, J. et al. 48-Gbit/s 8K video-transmission using resonant tunnelling diodes in 300-GHz band. *Electron. Lett.* **57**, 668–669 (2021).

28. Yoshioka, T. et al. 48-Gbit/s 8K video-transmission using frequency-division multiplexing in 300-GHz band. in *2022 Asia-Pacific Microwave Conference (APMC,2022)*, 46-48 (Yokohama, 2022).

29. Wang, C. et al. 0.34-THz wireless link based on high-order modulation for future wireless local area network applications. *IEEE Trans. Terahertz Sci. Technol.* **4**, 75–85 (2014).

30. Wang, C. et al. A 10-Gbit/s wireless communication link using 16-QAM modulation in 140-GHz band. *IEEE Trans. Micro. Theory Tech.* **61**, 2737–2746 (2013).

31. Morishita, Y. et al. 300-GHz-Band OFDM video transmission with CMOS TX/RX modules and 40dBi Cassegrain antenna toward 6G. *IEICE Trans. Electron.* **E104.C**, 576–586 (2021).

32. Devlin, B. et al. Reports from the SMPTE technology committees. *MPTE Motion Imaging J.* **129**, 10–20 (2020).

33. R. P. ITU-R, 676-13, Attenuation by atmospheric gases and related effects, Geneva, Switzerland, 2022.

34. Ericsson blog, 5G energy consumption: what's the impact of 5G NR in real networks? https://www.ericsson.com/en/blog/2021/10/5g-energy-consumption-impact-5g-nr (2021).

35. Saha, S., Siddiqui, T., Koutsonikolas, D., Loch, A., & Widmer, J. A detailed look into power consumption of commodity 60 GHz devices. *IEEE 18th International Symposium on A World of Wireless, Mobile and Multimedia Networks*, 1–10, (2017).

36. Goldsmith, A. *Wireless Communications*. (Cambridge Univ. Press, London, 2005).

37. Saadat, A., Salman, M. & Saadta, H. Matched filter based timing synchronization for orthogonal frequency division multiplexing systems. in *2013 IEEE 8th Conference on Industrial Electronics and Applications (ICIEA,2013)*, 1156-1161 (Melbourne, 2013).

38. Rezola, A. et al. Built-in-self-calibration for I/Q imbalance in wideband millimeter-wave gigabit transmitters. *IEEE Trans. Micro. Theory Tech.* **65**, 4758–4769 (2017).

39. Zhang, H., Huang, X., Zhang, T., Zhang, J. & Guo, Y. A 30 Gbps low-complexity and real-time digital modem for wireless communications at 0.325 THz. in *2019 19th International Symposium on Communications and Information Technologies (ISCIT, 2019)*, 260–264 (Ho Chi Minh City, 2019).

40. Feng, Y. et al. WR-2.8 band pseudoelliptic waveguide filter based on singlet and extracted pole resonator. *IEEE Access* **7**, 54705–54711 (2019).

Acknowledgements

Author contributions

Competing interests

The authors declare no competing interests.

Additional information

Supplementary information The online version contains supplementary material available at https://doi.org/10.1038/s41467-024-52370-x.

Correspondence and requests for materials should be addressed to Yinian Feng, Chong Han, Zhi Chen or Bo Zhang.

Peer review information *Nature Communications* thanks the anonymous reviewer(s) for their contribution to the peer review of this work. A peer review file is available.

Reprints and permissions information is available at http://www.nature.com/reprints

Publisher's note Springer Nature remains neutral with regard to jurisdictional claims in published maps and institutional affiliations.